Polymer 49 (2008) 3327–3334

Contents lists available at ScienceDirect

Polymer

journal homepage: www.elsevier.com/locate/polymer

The effects of the selectivity of the toluene/ethanol mixture on the micellar and the ordered structures of an asymmetric poly(styrene-*b*-4-vinylpyridine)

Soo-Young Park*, Woo-Hwan Sul

Department of Polymer Science, Kyungpook National University, #1370 Sangyuk-dong, Buk-gu, Daegu 702-701, Republic of Korea

ARTICLE INFO

Article history:
Received 15 March 2008
Received in revised form 5 May 2008
Accepted 18 May 2008
Available online 23 May 2008

Keywords:
Poly(styrene-*b*-4-vinylpyridine)
Solvent selectivity
Toluene and ethanol mixtures

ABSTRACT

The effects of the solvent selectivity of toluene/ethanol mixtures on the micellar and ordered structures of an asymmetric diblock copolymer of PS(19.6 K)-*b*-P4VP(5.1 K) in the dilute (1 wt%) and semi-dilute (8 wt%) solutions, as well as in the gel and solid films, were studied using small angle X-ray scattering (SAXS), generalized indirect Fourier transform (GIFT), and transmission electron microscopy (TEM) methods. The solvent selectivity was controlled by ϕ (weight percentage of ethanol in toluene/ethanol mixture). Individual micelles, space-filled micellar structure (without three-dimensional order), and three-dimensionally ordered gel and solid structures were observed from the 1 and 8 wt% solutions, the gel, and the solid film, respectively. In the 1 wt% solution, the individual micellar structures were strongly dependent on ϕ; the spherical micelles with P4VP core at $\phi = 0$, the unimer state at $10 \leq \phi \leq 50$, the spherical micelles with PS core at $\phi = 60$, the cylindrical micelles with PS core at $\phi = 70$ and 80, and precipitation at $\phi = 90$ and 100 were observed. The 8 wt% solution was close to overlap concentration with the unimer state in the regions of $20 \leq \phi \leq 40$. In the gel, the ordered structure was observed in the sequence of bcc, hexagonal, gyroid, lamellar, reverse hexagonal and random as ϕ increased, and could be explained by the change of the relative volume fraction of each block as ϕ changed, similar to the phase sequence in the phase diagram of the diblock copolymer. The solid films showed the various kinetically frozen ordered microstructures such as randomly packed sphere, hexagonal, gyroid, hexagonally perforated lamella, reversed hexagonal, and randomly packed cylinder, which were controlled by the solvent quality in the gel before solidification. We believe that these results can be applied to photonic crystals, self-assembled nano-patterning, and functional nanoparticles in which the structural control is most important.

1. Introduction

Block copolymers are able to self-assemble to characteristic morphologies in bulk and to micelles in selective solvents [1,2]. The micelles in selective solvents consist of core and surrounding protective corona, which are formed by insoluble and soluble chains, respectively. The morphologies are mainly controlled by a force-balance arising from stretching of the core chains, repulsive interactions between the corona chains, and surface tension at the core/corona interface [3,4]. This force-balance is a function of several variables such as the block copolymer composition and concentration [4], the type and concentration of added ions [5,6], and the solvent selectivity [3,7]. The block–block interaction parameter, χ, the molecular weight, and the composition of each block are the major factors governing the force-balance and in turn, the morphologies in the bulk as well as in the solution states. Intrinsic properties such as χ, the molecular weight, and the composition of each block play important roles in balancing these force contributions, and they are not readily tunable factors for a given system. However, the solvent selectivity can be adjusted relatively easily and causes a large effect on the morphologies of the micelles.

"Crew-cut" micelles can be formed when corona chains are much shorter than core ones, and "hairy" micelles can be formed when the relative lengths are reversed. A sphere-to-cylinder-to-lamella (or vesicle) transition is sometimes observed from the crew-cut micelles by increasing solvent selectivity, although usually spherical micelles are observed in the hairy micelles. The size of the core is known to increase as solvent selectivity increases in order to reduce the surface tension, so the core chains are stretched in the radial direction compared with their dimensions in the unperturbed state [4]. The degree of stretching is likely proportional to the radius of the micelle core [8,9]. This stretching of the core chains decreases as the shape changes from sphere (the ratio of the core radius to the chain end-to-end distance in the unperturbed state, $r = 1.4$), to rod ($r = 1.25$), and to lamella (or vesicle) ($r = 1.0$). Beyond a certain degree of stretching, the morphology changes

* Corresponding author. Tel.: +82 53 950 5630; fax: +82 53 950 6623.
E-mail address: psy@knu.ac.kr (S.-Y. Park).

0032-3861/$ – see front matter © 2008 Elsevier Ltd. All rights reserved.
doi:10.1016/j.polymer.2008.05.028

from sphere to rod, and eventually to lamella (or vesicle), presumably in order to reduce the thermodynamic stretching penalty. However, the repulsive interactions among the corona chains increase as the morphology changes from sphere to rod and to lamella due to the increasing crowdedness between the corona chains. For crew-cut micelles, the increase of repulsive interactions in the corona would be smaller than the decrease of stretching energy due to short corona chain length. Thus, more morphological changes can be expected from the crew-cut micelles than the hairy micelles by changing solvent selectivity.

The pioneering works for controlling the block copolymer morphology through solvent selectivity variation have been done by the Eisenberg group, who investigated poly(styrene-*b*-acrylic acid) (PS-*b*-PAA) ionic diblock copolymers in mixtures of water/dioxane or water/dimethylformamide (DMF) [10–14]. The solvent selectivity was adjusted by adding water through dialysis. A sphere-to-cylinder-to-vesicle transition was achieved by increasing the fraction of water (solvent selectivity) in the mixture. Lodge et al. also studied asymmetric poly(styrene-*b*-isoprene) (PS-*b*-PI) solutions in a series of solvent mixtures of dibutyl phthalate (DBP), diethyl phthalate (DEP), and dimethyl phthalate (DMP). They also found that the predominant micellar shape changes from sphere to cylinder and to vesicle as the solvent selectivity increased [15]. We also studied the PI cross-linked micelles of the asymmetric PS-*b*-PIs in the DBP/DEP/DMP mixtures and found similar transitions. In that study, the giant vesicular micelles (diameter of $\sim$2.5 μm) were observed in high selectivity solvents through TEM images [16]. However, the solvents for solvent-selectivity control were usually the mixtures of neutral and selective solvents. Recently, we reported the micellar and ordered structures of a symmetric PS(12 K)-*b*-P4VP(11.8 K) in the binary solvent mixtures of toluene (PS selective solvent) and ethanol (P4VP selective solvent) in the dilute, semi-dilute, and concentrated solutions as well as in the solid state [17,18]. Because toluene and ethanol are selective to opposing blocks, mixtures of the solvents range from the one-block selective, to neutral, to the other-block selective solvents. By mixing these two selective solvents, the various structures for PS(12 K)-*b*-P4VP(11.8 K) such as hard/soft spherical micelles in the dilute solution, fcc (face centered cubic), bcc (body centered cubic), and hexagonal packing in the concentrate solution were observed.

In this article, we will report on the micellar as well as the solid-state structures of an asymmetric PS(19.6 K)-*b*-P4VP(5.1 K) in toluene/ethanol mixtures in order to clarify not only the influence of the block selective solvent but also the effects of the block copolymer asymmetry on the morphologies of the resulting micelles and the final solid-state structures. In this system, blocks forming the core and corona reverse positions in one pure solvent with respect to the other pure solvent. Because of the asymmetry of PS(19.6 K)-*b*-P4VP(5.1 K), a broad range of morphologies were achieved by changing solvent selectivity. This was previously only achievable by changing the composition of the block copolymer.

2. Experimental

2.1. Samples

PS-*b*-P4VP was purchased from Polymer Source©, Inc. (Canada) which had been synthesized by an anionic polymerization method. Toluene and ethanol were used as selective solvents for the PS and P4VP blocks, respectively. Two solvents were miscible and mixed in varying proportions in order to control the selectivity of the solvent [19]. The weight percentage of ethanol in the mixture was denoted as ϕ. The solution samples were prepared by direct dissolution of polymers in the solvent. The number-average molecular weight was 19 600/5100 (PS/P4VP) (PS(19.6 K)-*b*-P4VP(5.1 K)) and the polydispersity was 1.08. The copolymer was dissolved in the solvent mixtures at several concentrations. The gel state was made at the concentration where the solution did not flow in an inverted vial by increasing the concentration little by little from the solution state. The solid film was prepared by drying the gel between Kapton films. The ultra-thin solid film was sectioned by ultramicrotome (Leica EM UC6). The TEM samples (Hitachi H-7600, 100 kV) were prepared by dropping the solutions onto a 200-mesh carbon coated copper grid, absorbing the solvent on a filter paper, and evaporating the excess solvent at room temperature. The samples on the grid were stained with I_2 and RuO_4 vapors for 90 and 30 min, respectively.

2.2. Small angle X-ray scattering (SAXS)

The sample holder for SAXS has a mica window for X-ray transmission. For liquids, solution was injected into the holder and then the hole was sealed with epoxy in order to prevent evaporation. The gel samples were situated between Kapton films during SAXS measurements. Before SAXS measurement, some gel samples were sheared between Kapton films, by hand, to get an oriented state. Solid films between Kapton films were placed into the sample holder after evaporation of the solvents in open air. Experiments were performed at beamline 4C1 (the Pohang Light Source, Korea), where a W/B4C double-multilayer monochromator delivered monochromatic X-rays that had a wavelength of 0.16 nm. A flat Au mirror was used to reject the higher harmonics from the beam. A MarCCD camera (Mar USA, Inc. CCD165) was used to collect the scattered X-rays. The sample-to-detector distance (sdd) was 3 m, which allowed the SAXS data to be obtained in a q range between 0.06 and 1.11 nm^{-1} (sdd = 3 m). The sdd was calibrated using SEBS (polystyrene-*block*-poly(ethylene-*ran*-butylene)-*block*-polystyrene).

2.3. Data analysis

The raw spectra were corrected by conventional procedures for the background of the solvent and sample cell and detector efficiency. Two-dimensional scattering spectra were azimuthally averaged. The measured intensity $I(q)$ can be expressed as the product of form ($F(q)$) and structure ($S(q)$) factors, although $S(q)$ is negligible for the dilute solution. The SAXS data were analyzed with GIFT software, which was developed by Glatter [20–26]. Both $F(q)$ and $S(q)$ were determined simultaneously within one procedure in GIFT. While $F(q)$ is absolutely model free, $S(q)$ is calculated within the Percus–Yevick approximation and is not model independent. The hard-sphere model was employed for $S(q)$, whereby the effective hard sphere radius (R_{HS}) and the effective volume fraction (η) are the parameters to be determined. The average structure factor ($S_{avg}(q)$) was employed in this study. A monomodal size distribution (μ), characterized as a Schulz distribution, was included for the $S_{avg}(q)$ calculations. The Fourier transformation of $I(q)$ yields the pair distance distribution function ($p(r)$) of a particle, which is a histogram of distances inside the particle weighted with the electron density differences. The shape of $p(r)$ allows for the determination of basic geometry (spherical, cylindrical, or planar), even for inhomogeneous particles. D_{max} is the maximum intra-particle distance and $d_{max} = \pi/q_{max}$ where q_{max} is the peak position in scattering pattern. D_{max} was determined as the value of r at which $p(r) = 0$. This methodology using indirect Fourier transformation has been described elsewhere [20–26].

3. Results and discussion

Fig. 1a shows the SAXS patterns of the PS(19.6 K)-*b*-P4VP(5.1 K) solutions in toluene ($\phi = 0$) as a function of q with different concentrations. The 1 wt% solution showed only a form factor due to

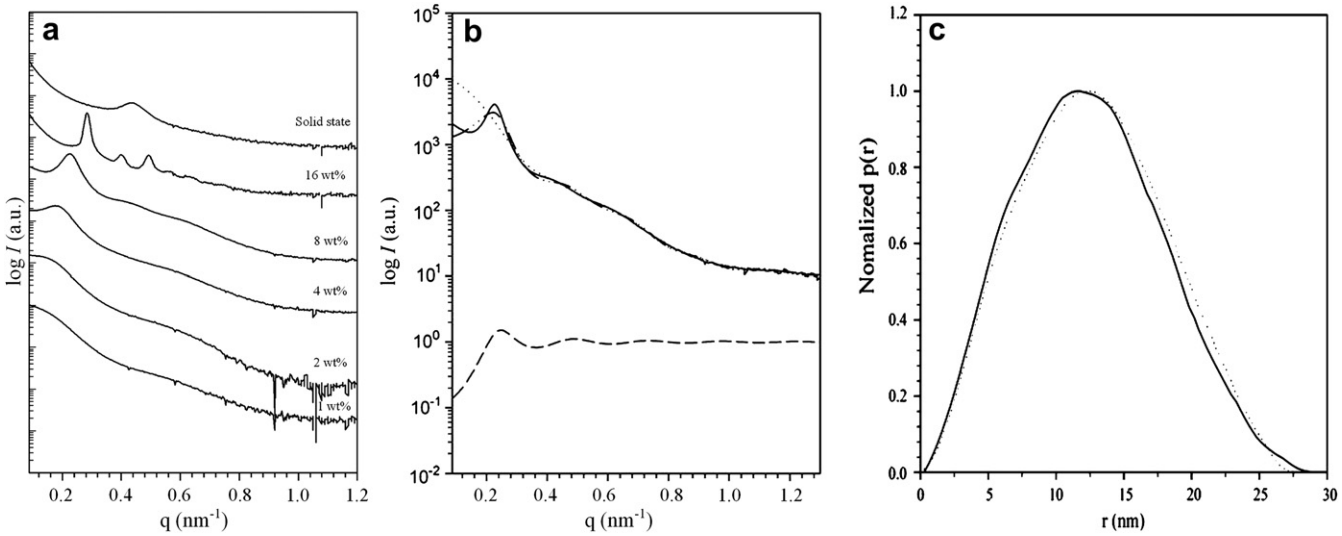

Fig. 1. (a) The SAXS patterns of the PS(19.6 K)-*b*-P4VP(5.1 K) solutions in toluene ($\phi = 0$) as a function of q with different concentrations; (b) the structure (————) and form (·····) factors, and the calculated (-···-) and observed (—) curves of the 8 wt% solution in toluene ($\phi = 0$); (c) the normalized $p(r)$s calculated from the 1 wt% solution in (a) (—), and the form factor of the 8 wt% solution in (b) (·····).

low concentration. The 2 wt% solution showed an intensity decrease and became flat at low q ($q < 0.2$ nm^{-1}) as compared to the 1 wt% solution. The 4 wt% solution showed a large decrease in intensity at low q, which caused a scattering peak at $q = 0.177$ nm^{-1} ($d = 35.5$ nm). This peak represents the average distance between the micelles in the solution and shifted to a higher q ($q = 0.226$ nm^{-1}, $d = 27.8$ nm) for the 8 wt% solution due to shorter distance between micelles. The 16 wt% sample showed several peaks at $q = 0.283$, 0.398, 0.491, 0.564, 0.633, and 0.746 nm^{-1} with bcc ratios of $1{:}\sqrt{2}{:}\sqrt{3}{:}\sqrt{4}{:}\sqrt{5}{:}\sqrt{6}{:}\sqrt{7}$. The calculated cubic unit cell dimension (a_{bcc}) is 31.5 nm. The closest distance between the micelles in the bcc unit cell ($D_{nn,bcc} = a \times \sqrt{3}/2$) is 27.2 nm. It is known that steep and short-range interactions (applicable to crew-cut micelles) favor fcc, whereas soft and long-range potentials (applicable to hairy micelles) favor bcc. The observation of the bcc unit cell might be due to the longer PS corona chains in toluene [27–35]. The SAXS in the solid state will be discussed in detail later. Fig. 1b shows, as an example, the separated form and structure factors, and the observed and calculated SAXS patterns of the 8 wt% solution in (a). The calculated SAXS pattern is a product of form and structure factors. The observed and calculated curves were close to each other, indicating that the form and structure factors were accurately separated from the observed SAXS pattern. Fig. 1c shows the normalized $p(r)$ distributions of the 1 and 8 wt% solutions. The $p(r)$ of the 1 wt% solution was calculated from the SAXS pattern (Fig. 1a, 1 wt%) while the $p(r)$ of the 8 wt% solution was calculated from the form factor (b). The two $p(r)$s were similar to each other, indicating that the basic hairy spherical micelle structure did not change with an increase in concentration from 1 to 8 wt%.

3.1. Dilute solutions

Fig. 2a shows the SAXS patterns of the 1 wt% solutions as functions of q and ϕ. The intensity at $\phi = 10$ decreased significantly from that at $\phi = 0$, and the decreased intensity continued until $\phi = 50$. The low intensity was probably due to the deterioration of the solvent selectivity and thus the unimer state of the block polymer in the solution; we could not analyze any micelle structures from the SAXS curves at $\phi = 10$–50. Although the intensity

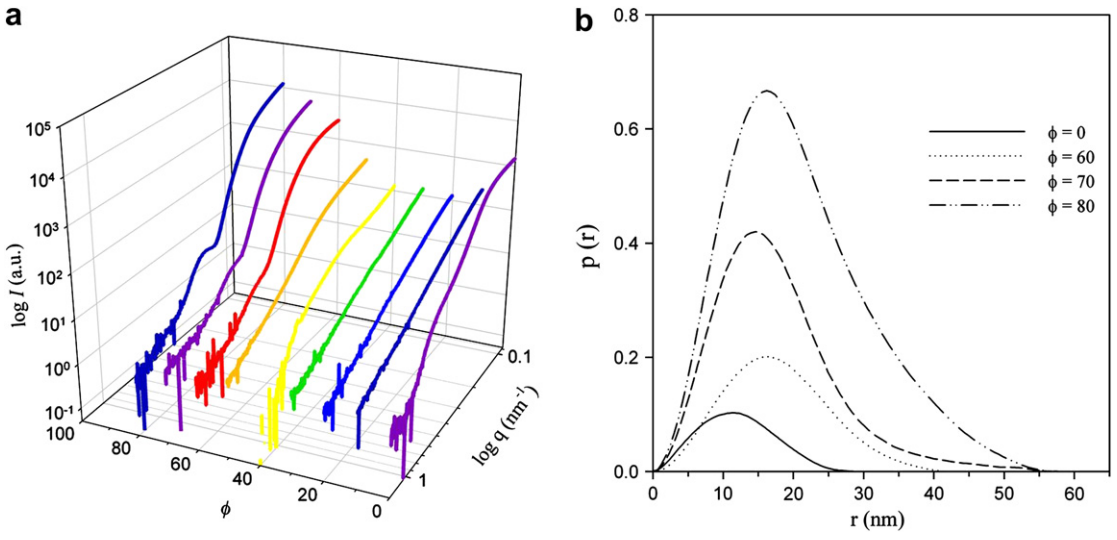

Fig. 2. (a) The SAXS patterns of the 1 wt% solutions as functions of q and ϕ; (b) the $p(r)$s at $\phi = 0$, 60, 70, and 80.

at $\phi = 50$ slightly increased, it was still ~100 times lower than that at $\phi = 0$. The intensity reappeared at $\phi = 60$–80, but the solutions at $\phi = 90$ and 100 became milky. The milky state occurred because PS(19.6 K)-*b*-P4VP(5.1 K) was not soluble in the ethanol-rich solvents (at $\phi = 90$ and 100) due to the short soluble chain length of P4VP. Asymmetry in the block length would cause the micelles in the toluene-rich and ethanol-rich solvents to be hairy and crew-cut, respectively, while the unimer state could be generated in the middle-mixing ratios. The hairy micelles with P4VP core were observed only at $\phi = 0$, while the crew-cut micelles with PS core were observed at the wider range of $\phi > 60$ (including the insoluble). This was because the short P4VP core chains in the hairy micelles have less capacity to maintain the micelle structure than the long PS core chains in the crew-cut micelles. Fig. 2b shows the $p(r)$s at $\phi = 0$, 60, 70, and 80. The shapes of $p(r)$s at $\phi = 0$ and 60 were typical of a sphere with D_{max} of 28 and 42 nm, respectively. The D_{max} at $\phi = 60$ (42 nm) increased as compared to that at $\phi = 0$ (28 nm) due to the reversed micelle structure with long PS core. This result suggests that the SAXS scattered mainly the core part, (otherwise the similar D_{max}s would be observed at $\phi = 0$ and 60) which is coincident with our previous report [17]. The $p(r)$s at $\phi = 70$ and 80 showed a long tail with increased intensity, which is typical of a long cylinder. Thus we found that the spherical micelles changed to the cylindrical ones by increasing ϕ from 60 to 70.

Fig. 3 shows the TEM images of the 0.0156 wt% solutions at $\phi = 0$, 60, 70, and 80, which were prepared by the evaporation of the solutions on the carbon coated copper grid and stained with RuO_4. This sample preparation method for TEM cannot control the concentration of the solution because it becomes dense during evaporation and the equilibrium structures cannot be observed due to the high evaporation speed of toluene and ethanol. Information about the kinds of micelles present in the solution, however, might be obtained because the TEM samples were prepared with very dilute solutions (0.0156 wt%), which might have little effect on the already-formed micelle during drying on the grid. The solution at $\phi = 0$ (Fig. 3a) and $\phi = 60$ (b) showed only spherical micelles which had P4VP and PS cores, respectively. The diameters of the spherical micelles were 11.3 and 28.8 nm, respectively, and were reduced as compared to the SAXS data due to drying. The increase of micelle size at $\phi = 60$ (as compared to that at $\phi = 0$) may be due to the long core chains which were more extended than corona chains. The solution at $\phi = 70$ (Fig. 3c) showed a mixture of spherical and cylindrical micelles, while only cylindrical micelles could be observed from the solution at $\phi = 80$ (d). Solvent selectivity increases from $\phi = 60$ to 80. The increase of the solvent selectivity caused high surface tension at the interface between core and corona. The structural change from spherical to cylindrical micelles can happen when the surface tension in spherical micelles is too high to persist and is reduced by transforming to cylindrical micelles. The further increase of solvent selectivity (such as $\phi = 90$ and 100) would create the vesicular micelle if possible. However, the decrease in the solubility of the block copolymer caused precipitation (or milky state). Thus, only the structural change from spherical to cylindrical micelles was found in the 1 wt% solutions by changing solvent selectivity.

3.2. Semi-dilute solutions

Fig. 4 shows the SAXS curves of the 8 wt% solutions as functions of q and ϕ. The intensity was low and flat in the regions of $20 \le \phi \le 40$, indicating that these regions were in the unimer state. The regions in the unimer state decreased from $10 \le \phi \le 50$ to $20 \le \phi \le 40$ by increasing the concentration from 1 to 8 wt%. Broad peaks were observed at $q_{max} = 0.226$ ($d_{first} = 27.8$ nm), 0.287 ($d_{first} = 21.9$ nm), 0.182 ($d_{first} = 34.5$ nm), and 0.146 ($d_{first} = 43.0$ nm) nm^{-1} for the solutions at $\phi = 0$, 10, 50 and 60, respectively. These peaks were due to appearance of the structure factor. The values of d_{first} at $\phi = 50$ and 60 were larger than those at $\phi = 0$ and 10, due to the reverse structure with longer PS core. The D_{max} for spherical micelle (at $\phi = 0$ and 60) was close to the d_{first}; the D_{max} and the d_{first} for the solution at $\phi = 0$ were both ~28 nm, and those for the solution at $\phi = 60$ were 42 and 43 nm, respectively. This closeness between the d_{first} and the D_{max} indicates that the micelles were almost space-filled in the 8 wt% solution.

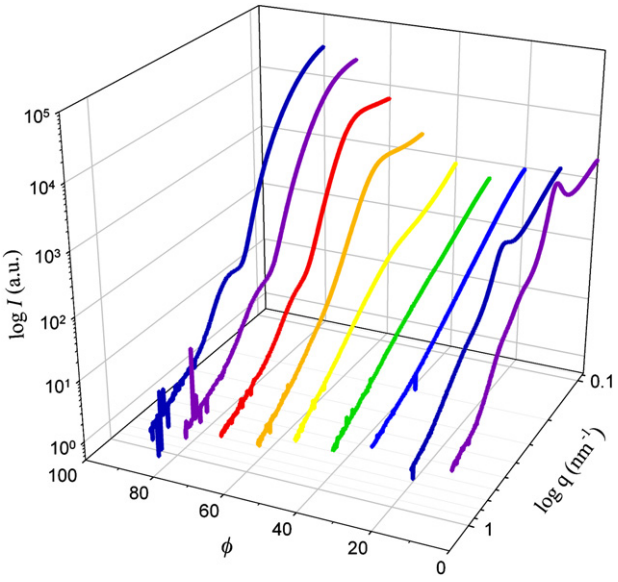

Fig. 4. The SAXS curves of the 8 wt% solutions as functions of q and ϕ.

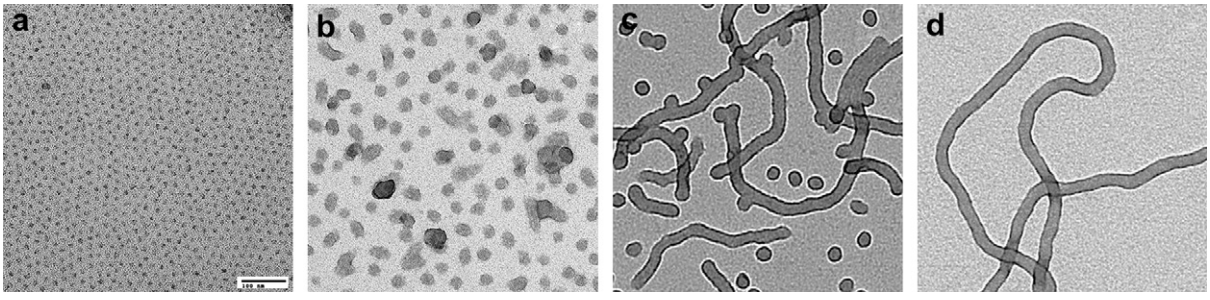

Fig. 3. TEM images of the 0.0156 wt% solutions at $\phi = 0$ (a), 60 (b), 70 (c), and 80 (d), which were prepared by the evaporation of the solutions on the carbon coated copper grid and stained with RuO_4; the magnification is all the same and the scale bar in (a) is for 100 nm.

3.3. Gel states

Block copolymers in the concentrated gel solution in a selective solvent can self-assemble into a variety of structures which are ordered on the mesoscopic length scale (i.e., typically 10-100 nm). In an AB diblock concentrated gel solution, ordered morphologies result from unfavorable interactions between A and B chain units, which often increase on lowering temperatures [29]. Fig. 5a shows the concentration of the solution at the beginning of gel state as a function of ϕ. The solutions at $\phi = 80$, 90, 100 became insoluble and milky before gel state was reached by increasing concentration. The gel state was confirmed when flow did not occur while the vial was inverted. The concentration at the beginning of the gel state was strongly dependent on ϕ. The shape of the curve is skewed with a maximum concentration at $\phi = \sim 30$. The regions at $20 \leq \phi \leq 40$ (which were unimer state in the 8 wt% solutions) needed higher concentrations to become a gel state than other regions. The gel was easily sheared between the Kapton films. Fig. 5b and c shows the two-dimensional SAXS patterns of the vertically sheared gel solutions and their azimuthally integrated one-dimensional curves as functions of q and ϕ, respectively. The SAXS patterns showed the several peaks in the gel state. The peak positions and their ratios before and after shearing are listed in Table 1. The SAXS curves were similar before and after shearing in terms of the ordered structure and the d-spacings of the observed peaks so that the SAXS patterns after shearing were discussed. The three-dimensionally ordered structures were generated even at ϕs of the unimer state in the 1 and 8 wt% solutions. The bcc symmetry was observed for the solutions at $\phi = 0$ and 10, indicating that the constituent unit was sphere. The a (and D_{nn}) of the bcc unit cell decreased as ϕ increased (the selectivity decreased) from 0 to 10 because the decrease of the selectivity caused the decrease of the aggregation number and the shrinkage of the corona chains. The

Table 1
Ratios of q/q_{1st} (q_{1st} is the first q value), the symmetries (bcc (body centered cubic), HEX (hexagonal), LAM (lamella)), the a dimension (in bcc, hexagonal, and lamella), the D_{nn} (the closest distance between micelle in the unit cell) with respect to ϕ for a PS(19.6 K)-*b*-P4VP(5.1 K) gel solution before (above in the raw) and after (below in the raw) shearing

ϕ	Ratios of q/q_{1st}	q_{1st} (nm^{-1})	Symmetry	a (nm)	D_{nn} (nm)
0	1:√2:√3:√4/√5	0.2809	bcc	31.7	27.5
	1:√2:√3:√4:√5:√6:√7	0.269	bcc	33.1	29.1
10	1:√2:√3	0.3326	bcc	26.8	23.2
	1:√2:√3:√4	0.3382	bcc	26.3	22.8
20	1:√3:2	0.3326	HEX	21.8	
	1:√3:2	0.3342	HEX	21.7	
30	1:1.15	0.3193	Gyroid	48.2[a]	
	1:1.15:√3:2	0.3116	Gyroid/HEX	49.3[a]/23.3	
40	1:2	0.2902	LAM	21.7[b]	
	1	0.2916	LAM	21.5[b]	
50	1:√3:2	0.2345	HEX	30.9	
	1:√3:2	0.2383	HEX	30.5	
60	1	0.1749	RANDOM		
		0.2117			
70	1	–	RANDOM		
		0.1811			
80–100	Precipitated				

[a] The a dimension of gyroid was calculated from indexing first two reflections as *211* and *220*, respectively.
[b] The a dimension of lamella was calculated from indexing the first peak as *100*.

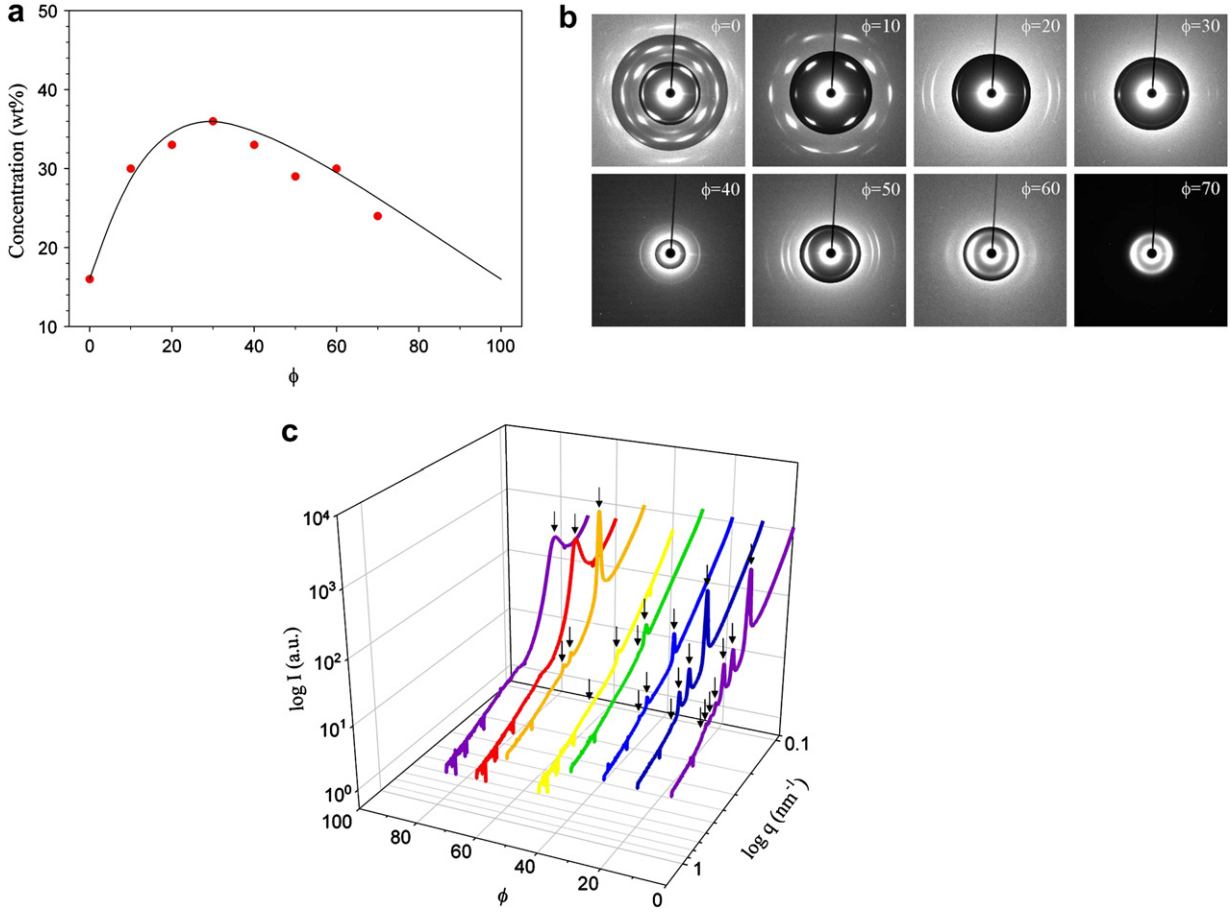

Fig. 5. (a) The concentration of the solution at the beginning of gel state as a function of ϕ; (b) two-dimensional X-ray patterns of vertically sheared gel solutions, the central part was adjusted in contrast for better view; (c) their azimuthally integrated SAXS scattering curves as functions of q and ϕ.

bcc symmetry was coincident with the reported results for the packing of the hairy micelles [18]. The solution at $\phi = 20$ (which was unimer state at the 1 and 8 wt%) showed equatorial peaks at $q = 0.334$, 0.581, and 0.670 nm^{-1} with the hexagonal ratios of $1:\sqrt{3}:2$. The core chain might still be P4VP because the a dimension of the hexagonal lattice (21.7 nm) at $\phi = 20$ is similar to the D_{nn} of the bcc lattice ($\sim$22.8 nm) at $\phi = 10$; the a dimension of the hexagonal lattice is the closest distance between two adjacent cylinders so that these two values can be compared. The solution at $\phi = 30$ shows the typical gyroid peaks at $q = 0.312$ and 0.360 nm^{-1} with the ratio of $1:\sqrt{(4/3)}$ (=1.15). This gyroid of PS-*b*-P4VP was observed for the first time due to our systematic screening of the solvent selectivity. This gyroid structure was also confirmed from TEM of the solid films (which will be discussed later). The solution at $\phi = 40$ shows two lamellar peaks at $q = 0.290$ and 0.583 nm^{-1} with the ratio of 1:2. Thus, the gyroid changed to lamella by increasing ϕ from 30 to 40. The hexagonal structure reappeared at $\phi = 50$ with three hexagonal peaks at $q = 0.238$, 0.414, and 0.475 nm^{-1} and their ratios of $1:\sqrt{3}:2$. The a dimension of hexagonal lattice at $\phi = 50$ (30.5 nm) increased as compared to that at $\phi = 20$ (21.7 nm) due to the reverse long PS core. The solutions at $\phi = 60$ and 70 show only broad peaks similarly to the 8 wt% solutions due to the absence of the long-range orders and the appearance of the structure factor. The sequence of the ordered structures proceeded as bcc, hexagonal, gyroid, and lamella as ϕ increased until 40. This sequence is the same as that in the phase diagram of the diblock copolymer as a function of volume fraction [36,37]. The standard parameters controlling AB diblock copolymer phase behavior in the melt are χN and f_A, where χ is an A–B segment interaction parameter, N is the overall degree of polymerization, and f_A is the volume fraction of the A block. The solvent quality for PS and P4VP decreases and increases, respectively, as ϕ increases so that PS chains shrink and the volume fraction of PS (f_{PS}) decreases (and P4VP chains will show reverse behaviors) as ϕ increases. This f_{PS} change in the gel by the change of the solvent selectivity is similar to that in the melt by the change of the block copolymer composition. Thus, we could find the same phase sequence of bcc, hexagonal, gyroid, and lamella in the gel state. The phase sequence of the symmetric diblock copolymer in the melt is symmetric against $f_A = 0.5$ so that we can expect another reverse sequence of lamella, reverse gyroid, reverse hexagonal, and reverse bcc as ϕ increases. However, we could find only reverse hexagonal at $\phi = 50$ with skipped reverse gyroid, and could not find reverse bcc due to the insolubility of the diblock copolymer at $\phi \geq 80$. The reverse gyroid could be found from narrower screen of ϕ. The broad peaks at $\phi = 60$ and 70 indicate the loss of the long-range orders between the unit structures and shifted from $q = 0.21$ to 0.18 nm^{-1} by increasing ϕ from 60 to 70. This decrease of the q value was due to more extended PS core chains at $\phi = 70$. The crew-cut micelles at $\phi = 60$ and 70 were cylindrical in the 1 wt% solution (as discussed in Fig. 2) so that the unit of disordered structure could be other than sphere (such as cylinder). This disordered structure will be discussed in Section 3.4.

3.4. Solid films

Fig. 6a and b shows the SAXS curves of the solid films which were prepared by drying the gel between Kapton films in the open air and their sectioned TEM micrographs, respectively. The structures in the solid films were not thermodynamically equilibrated but kinetically frozen from the gel by drying. The purpose of this study was to elucidate the structural control of a diblock copolymer by changing solvent quality in the gel although the generated structure is not in thermodynamically equilibrium. The bcc peaks in the gel at $\phi = 0$ became a broad peak at $q = 0.425$ nm^{-1}, indicating that the bcc structure lost long-range orders and became a randomly packed structure during drying (the detail structural change during drying will be discussed in Fig. 6c). Similar to those at $\phi = 0$, the bcc peaks at $\phi = 10$ became a broad peak at $q = 0.385$ nm^{-1}. These randomly packed spherical micelles were also found in the TEM micrograph at $\phi = 10$ (Fig. 6b-i) in which average distance between micelles was 15.7 nm and was close to the d-spacing of the broad peak ($d = 16.4$ nm) in SAXS. The hexagonal structure was observed at $\phi = 20$, which was evident from the SAXS pattern (Fig. 6a, $\phi = 20$) as well as from the TEM micrograph (b-ii). The a dimension was $\sim$24.2 nm in both experiments. The SAXS at $\phi = 30$ shows the gyroid peaks at $q = 0.288$, and 0.311 nm^{-1} with a ratio of 1:1.15. We also found the typical gyroid TEM images (Fig. 6b-iii, vi) which are similar to the reported ones [38,39]. Fig. 6b-iii represents the [110] projection of the gyroid unit cell and b-iv shows a mixture of different projections including a "wagon-wheel image". This gyroid structure of PS-*b*-P4VP was for the first time observed to our knowledge and can be applied to many applications such as photonic crystals. The calculation of photonic properties showed that the gyroid structure is a desirable and very effective morphology for making photonic crystals [40]. The solid films at $\phi = 40$ show several peaks at $q = 0.236$, 0.280, 0.470, and 0.701 nm^{-1}. Among them, the peaks at $q = 0.236$, 0.470, 0.701 nm^{-1}

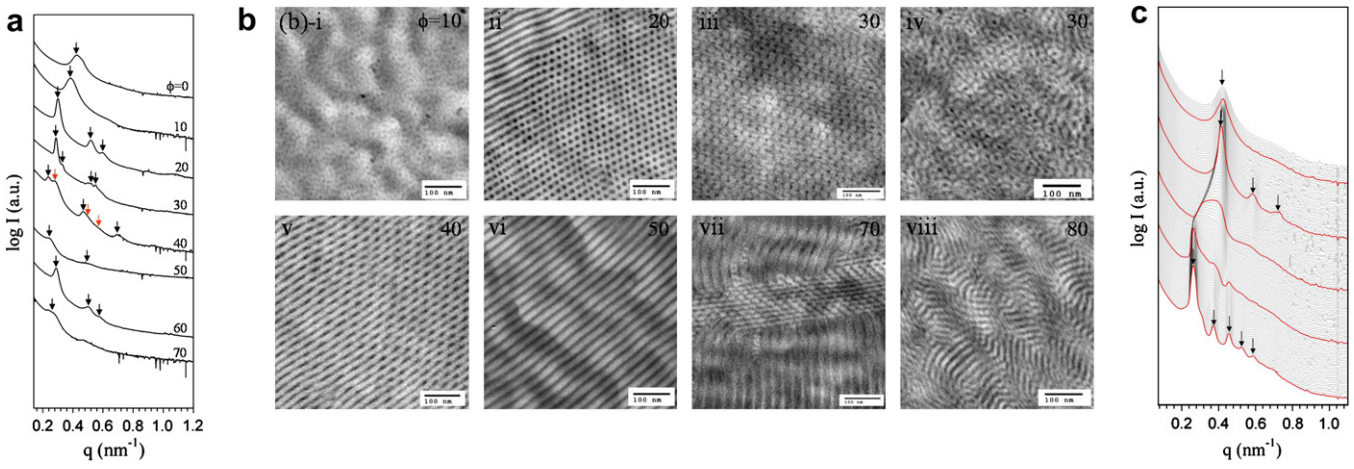

Fig. 6. (a) The SAXS patterns of the solid films which were prepared by drying the gel solutions; (b) TEM micrographs of the sectioned films at the different ϕs; (c) the change of the SAXS pattern at $\phi = 0$ during drying from the gel (16 wt% solution) to the solid film; the bold line represents 175 s interval. (For interpretation of the references to colour in this figure legend, the reader is referred to the web version of this article.)

(shown in black arrows) were 1:2:3. The position of the peak at $q = 0.280\ nm^{-1}$ (shown in red arrows) was similar to that of the hexagonal peak at $\phi = 60$ (will be discussed later), and their hexagonal traces of *110* and *200* at $q = 0.485$, and $0.558\ nm^{-1}$ (shown in red arrows) were also found. The existence of both lamellar and hexagonal peaks indicates the hexagonally perforated lamellar (HPL) phase with dimensions of $a = 25.9$ and $c = 26.7$ nm. The typical HPL images were also observed in Fig. 6-v [41,42]. The distance between the layers was 21.5 nm and that between the spheres in the layer was 19.3 nm. These values were a little smaller than SAXS data because the sectioning direction might be not completely normal to the lamellar plane. The solid film at $\phi = 50$ shows the peaks at $q = 0.248$, $0.495\ nm^{-1}$ with a ratio of 1:2, indicating that the lamellar structure with a repeat of 25.3 nm was generated. The lamellar structure was also observed from the TEM micrograph at $\phi = 50$ (Fig. 6b-vi) showing clear regular alternating layers consisting of PS and P4VP blocks with a repeat of 24.6 nm which was close to the SAXS result (25.3 nm). The solid film at $\phi = 60$ showed the hexagonal peaks at $q = 0.288$, 0.501, and $0.580\ nm^{-1}$ with the ratios of $1:\sqrt{3}:2$. This hexagonal structure, however, was reverse hexagonal with PS core as compared to that at $\phi = 20$. The TEM micrograph (Fig. 6b-vii) also showed the hexagonal structure with PS core, which was evident from the misaligned part in the middle of figures; the core is whiter than the outside corona as compared to that at $\phi = 20$, which showed more black in the core (b-ii). The solid film at $\phi = 70$ showed only broad peaks as compared to those at $\phi = 60$, indicating loss of the long-range orders. We also found randomly packed cylinders in Fig. 6b-viii. The average distance between cylinders of 22.8 nm was close to the *d*-spacing of the broad peak in SAXS (23.8 nm). Thus the unit random structure at $\phi = 70$ was cylinder as compared to sphere at $\phi = 0$ and 10. Fig. 6c shows the change of SAXS scattering curves at $\phi = 0$ during drying from the gel (16 wt% solution) to solid state. The bold line represents 175 s interval. The initial bcc reflections (which are the same as the reflections of the gel state in Fig. 5) became weak and diffuse, and thus, decreased in the number of the observed reflections during the initial drying. The first main peak at $q = 0.25\ nm^{-1}$ became weak, continuously shifted to a wider angle after $t = 300$ s, and combined with a new broad peak at $q = \sim 0.42\ nm^{-1}$ to become a diffuse reflection. However, the combined peak at $q = \sim 0.42\ nm^{-1}$ became intense and sharp with additional peaks at $q = 0.59$ and $0.73\ nm^{-1}$, and the initial peak at $q = 0.25\ nm^{-1}$ disappeared completely after $t = 500$ s. The new peaks might be from the dried micelles. The sample could be dried first at the surface but remains wet inside the sample until complete drying occurred. The continuous shift of the peaks at $q = 0.25$ to $\sim 0.4\ nm^{-1}$ indicated that the micelles progressively shrank to the dried state. The absence of high ordered reflections and the broadness of the peak during the initial drying indicate the loss of the packing order. The shrinkage in the corona chains did not happen simultaneously for the whole part of the sample during the initial drying. The order of packing was regenerated after $t = 700$ s, which is evident from the appearance of the high order reflections at $q = 0.59$ and $0.73\ nm^{-1}$. The size of the micelle became uniform again after complete shrinkage in the corona. The peaks were observed at $q = 0.418$, 0.594, and $0.726\ nm^{-1}$ and their ratios are $1:\sqrt{2}:\sqrt{3}$, indicating bcc symmetry. The calculated cubic unit cell dimension ($a_{bcc,dried}$) is 21.2 nm. The closest distance between the micelles for the dried bcc unit cell ($D_{nn,bcc,dried}$) is 18.4 nm. The ratio between a_{bcc} and $a_{bcc,dried}$ ($D_{nn,bcc}$ and $D_{nn,bcc,dried}$) is 1.49. This large decrease of the *a* dimension is mainly due to the condensed corona chain; the corona chains contained a lot of solvents as compared to the core chains which are similar to a solid state in a highly selective solvent. However, the long-range interactions among the micelles were much reduced and the packing order of the micelle was lost again after some time, as indicative of re-disappearance of the high ordered peak and only one broad peak remaining at $q = 0.422\ nm^{-1}$ in the solid state. This random structure was due to the completely collapsed corona chains, which cause only the short-range orders (without long-range order). From this in situ dynamic drying SAXS experiments, we could monitor the drying process and find another shrinking bcc unit cell and random structure.

We could control the ordered structures in the solid film of an asymmetric PS(19.6 K)-*b*-P4VP(5.1 K) by simply changing solvent quality in the gel state through mixing two selective solvents. These findings suggest that control of solvent selectivity in the gel paves a way to study more diverse ordered structures. Another import aspect we found was how to control kinetically frozen structures during drying. We dried the gel in open air in this study but we also found significant difference of the ordered structures when the samples were dried in a vacuum oven for fast drying. We are now focusing on this aspect by adapting more controllable experimental conditions during drying and will report when the results are ready.

4. Conclusions

The effects of the solvent selectivity on the micellar and the three-dimensionally ordered structures of an asymmetric PS(19.6 K)-*b*-P4VP(5.1 K) diblock copolymer were narrowly screened by using toluene/ethanol mixture. We found significant structural difference in the micellar, gel, and solid states depending on ϕ. In the 1 wt% solution, the hairy spherical micelle with P4VP core at $\phi = 0$, the unimer state at $10 \leq \phi \leq 50$, the spherical micelles with PS core at $\phi = 60$, the cylindrical micelles with PS core at $\phi = 70$ and 80, and precipitation at $\phi = 90$–100 were observed. The 8 wt% solution was close to overlap concentration with the unimer state in the regions of $20 \leq \phi \leq 40$. In the gel, the three-dimensionally ordered structures were observed. The sequence of the ordered structure was bcc, hexagonal, gyroid, lamellar, reversed hexagonal, and random as ϕ increased. This sequence could be explained by the change of volume fraction as ϕ (solvent quality) changed, similar to the phase diagram of the symmetric diblock copolymer. The solid films were made from the gel by drying them in open air. The kinetically frozen structures in the solid films such as randomly packed sphere, hexagonal, gyroid, hexagonally perforated lamella, reversed hexagonal, and randomly packed cylinder were discovered with an asymmetric block copolymer. These findings might suggest that the control of solvent selectivity in the gel paves a way to study more diverse ordered structures from narrowly screening the solvent selectivity. We believe that more systematic structural changes can be possible with more narrow solvent mixture ratios and different solvent mixture systems and these results can be applied to photonic crystals, self-assembled nano-patterning, and functional nanoparticles in which the structural control is most important.

Acknowledgements

This work was supported by a 2007 NBIT program from MOST and AFOSR. And synchrotron work was supported in part by the Ministry of Science & Technology (MOST), by POSCO, by the Center for Integrated Molecular System (Korea Science & Engineering Foundation), by the KISTEP (Basic Research Grant of Nuclear Energy, MOST).

References

[1] Hadjichristidis N, Pispas S, Floudas G. Block copolymers. Synthetic strategies, physical properties and applications. New York: Wiley; 2003.
[2] Tuzar Z, Kratochvil P. Adv Colloid Interface Sci 1978;6:201.

[3] Yu Y, Eisenberg A. J Am Chem Soc 1997;119:8383.
[4] Zhang L, Eisenberg A. Science 1995;268:1728.
[5] Zhang L, Eisenberg A. Macromolecules 1996;29:8805.
[6] Van der Maarel JRC, Groenewegen W, Egelhaaf SU, Lapp A. Langmuir 2000;16:7510.
[7] Ding J, Liu G. Macromolecules 1999;32:8413.
[8] Whitemore MD, Noolandi J. Macromolecules 1985;18:657.
[9] Nagarajan R, Ganesh K. J Chem Phys 1989;90:5843.
[10] Shen H, Eisenberg A. J Phys Chem B 1999;103:9473.
[11] Chen L, Shen H, Eisenberg A. J Phys Chem B 1999;103:9488.
[12] Zhang L, Eisenberg A. Macromolecules 1999;32:2239.
[13] Shen H, Eisenberg A. Macromolecules 2000;33:2561.
[14] Choucair A, Eisenberg A. Eur Phys J E 2003;10:37.
[15] Bang J, Jain S, Li Z, Lodge TP, Pedersen JS, Kesselman E, et al. Macromolecules 2006;39:1199.
[16] Park S-Y, Park MH. Langmuir 2007;23:6788.
[17] Park S-Y, Chang YJ, Farmer BL. Langmuir 2006;22:11369.
[18] Park S-Y, Sul W-H, Chang YJ. Macromolecules 2007;40:3757.
[19] Available from: <http://www.sanderkok.com/techniques/hplc/micibility.html>.
[20] Glatter O, Krathy O. Small-angle X-ray scattering. London: Academic Press; 1982. p. 126.
[21] Glatter O. J Appl Crystallogr 1997;10:415.
[22] Glatter O. J Appl Crystallogr 1980;13:577.
[23] Glatter O. J Appl Crystallogr 1981;14:101.
[24] Brunner-Popela J, Glatter O. J Appl Crystallogr 1997;30:431.
[25] Bergmann A, Fritz G, Glatter O. J Appl Crystallogr 2000;33:1212.
[26] Weyerich B, Brunner-Popela J, Glatter O. J Appl Crystallogr 1999;32:197.
[27] Borisov OV, Zhulina EB. Macromolecules 2003;36:10029.
[28] Zhou Z, Li Z, Ren Y, Hillmyer MA, Lodge TP. J Am Chem Soc 2003;125:10182.
[29] Hamley IW. The physics of block copolymers. Oxford: Oxford University Press; 1998.
[30] Band J, Lodge TP. J Phys Chem B 2003;107:12071.
[31] McConnell GA, Alice PG, John SH, Steven DS. Phys Rev Lett 1993;71:2102.
[32] McConnell GA, Gast AP. Macromolecules 1997;30:435.
[33] Hamely IW, Pople JA, Diat O. Colloid Polym Sci 1998;276:446.
[34] Hamely IW, Daniel C, Mingvanish W, Mai SM, Booth C, Messe L, et al. Langmuir 2000;16:2508.
[35] Bang J, Lodge TP, Wang X. Phys Rev Lett 2002;89:215505.
[36] Matsen MW, Bates FS. J Polym Sci Polym Phys 1997;35:945.
[37] Matsen MW, Bates FS. Macromolecules 1996;29:1091.
[38] Suzuki J, Seki M, Matsushita Y. J Chem Phys 2000;112:4862.
[39] Avgeropoulos A, Dair BJ, Hadjichristidis N, Thomas EL. Macromolecules 1997;30:5634.
[40] Maldovan M, Urbas AM, Yufa N, Carter WC, Thomas EL. Phys Rev B Condens Matter Mater Phys 2002;65:165123/1–165123/5.
[41] Thomas EL, Anderson DM, Henkee CS, Hoffman D. Nature 1988;334:598.
[42] Spontak RJ, Smith SD, Ashraf A. Macromolecules 1993;26:956.